agriculture

MDPI

Article

Assessing Climate Change Effects on Winter Wheat Production in the 3H Plain: Insights from Bias-Corrected CMIP6 Projections

Yifei Xu [1], Te Li [2,*], Min Xu [1,*], Ling Tan [3] and Shuanghe Shen [4]

1 Jiangsu Climate Center, Nanjing 210018, China; xuyifeigov@126.com
2 Jiangsu Meteorological Observatory, Nanjing 210018, China
3 College of Economics and Management, Nanjing Agricultural University, Nanjing 210095, China; tanling_0902@163.com
4 School of Applied Meteorology, Nanjing University of Information Science & Technology, Nanjing 210044, China; yqzhr@nuist.com
* Correspondence: lite_nju@smail.nju.edu.cn (T.L.); amin0506@163.com (M.X.)

Abstract: Climate change exerts significant impacts on regional agricultural production. This study assesses the implications of climate change on winter wheat yields in the Huang-Huai-Hai Plain (3H Plain), utilizing bias-corrected climate projections from the Coupled Model Intercomparison Project Phase 6 (CMIP6) for mid-21st century (2041–2060) and late 21st century (2081–2100) periods under two shared socioeconomic pathways (SSP2–4.5 and SSP5–8.5). These projections were incorporated into the decision support system for agrotechnology transfer (DSSAT) CERES-Wheat model to forecast potential alterations in winter wheat production. Initial findings reveal that uncorrected CMIP6 projections underestimated temperature and precipitation while overestimating solar radiation across the southern 3H Plain. Following bias correction through the equidistant cumulative distribution function (EDCDF) method, the regional average biases for temperature, precipitation, and solar radiation were reduced by 18.3%, 5.6%, and 30.7%, respectively. Under the SSP2–4.5 and SSP5–8.5 scenarios, mid-21st century simulations predicted a 13% increase in winter wheat yields. Late 21st century projections indicated yield increases of 11.3% and 3.6% under SSP2-4.5 and SSP5-8.5 scenarios, respectively, with a notable 8.4% decrease in yields south of 36° N under the SSP5-8.5 scenario. The analysis of climate change factors and winter wheat yields in the 3H Plain under both scenarios identified precipitation as the key contributing factor to yield increases in the northern 3H Plain, while temperature limitations were the primary constraint on yields in the southern region. Consequently, adaptive strategies are essential to mitigate climate change impacts, with a particular focus on addressing the challenges posed by elevated temperature in the southern 3H Plain.

Keywords: CMIP6; DSSAT; climate change; winter wheat yield; projection

Citation: Xu, Y.; Li, T.; Xu, M.; Tan, L.; Shen, S. Assessing Climate Change Effects on Winter Wheat Production in the 3H Plain: Insights from Bias-Corrected CMIP6 Projections. *Agriculture* **2024**, *14*, 469. https://doi.org/10.3390/agriculture14030469

Academic Editor: Marcus Randall

Received: 4 February 2024
Revised: 6 March 2024
Accepted: 7 March 2024
Published: 13 March 2024

1. Introduction

In response to the escalating challenges posed by future climate change to agricultural production—challenges that are particularly acute in developing countries reliant on staple crops—the importance of related studies becomes evident [1–4]. Such challenges include increased evapotranspiration and agricultural water demand due to rising temperatures [5], exacerbating water scarcity in some regions and thus threatening agricultural productivity and food security [6].

In China, the past few decades have seen alterations in plant phenological events due to climate change, affecting critical agricultural timelines such as sowing and crop maturity dates [7]. This is particularly evident in the Huang-Huai-Hai Plain (3H Plain), China's leading wheat production area. Here, the irregular distribution of annual rainfall throughout the winter wheat's growing season could heighten drought risks [8], potentially leading to reduced yields [9]. Given the anticipated complexities of future climate change, it becomes imperative to explore its prospective impacts on winter wheat cultivation in the

3H Plain. Undertaking such investigations is crucial for safeguarding food security and fostering the sustainable development of agriculture.

Process-based crop models are extensively used to assess the potential impacts of climate change on winter wheat production and growth rates [10–12]. Among these, the decision support system for agrotechnology transfer (DSSAT) CERES-Wheat model stands out for its widespread application in analyzing climate change effects on crop yield [13–15], growth period [16,17], climate suitability [18,19], and agricultural planning [10,20]. The DSSAT CERES-Wheat model has demonstrated strong adaptability in China [21]. For example, the impacts of planning date shifts on the phenology of double cropping rice was determined by changing the planning date in the DSSAT CERES-Wheat model [22]. Xu et al. [23] analyze the effects of Pacific decadal oscillation (PDO) on winter wheat yields by using the DSSAT CERES-Wheat model and found that when PDO was in the positive (negative) phase, winter wheat yields tended to increase (decrease).

Global climate models (GCMs), especially those from the Coupled Model Intercomparison Project Phase 6 (CMIP6), play a crucial role in simulating future agricultural changes under various scenarios [10,24]. The CMIP6, with its advanced models and processes [25–28], has demonstrated a superior ability to capture large-scale climatological spatial distributions compared to previous generations of GCMs [29]. Recent assessments of CMIP6′s capability to accurately represent China's climate have shown improvements in the simulation of mean temperature and precipitation [30–32]. Projections for China's climate toward the end of the 21st century indicate annual increases in both temperature and precipitation [32–35], with the discrepancies in mean temperature across different scenarios becoming significantly pronounced over the long term [35].

Despite significant enhancements in CMIP6′s climatological variables for China, inaccuracies in temperature, precipitation, and radiation persist [27,36,37]. Accuracy is pivotal in making reliable climate forecasts and understanding climate change impacts on crop yields, as inaccuracies in climate projections are among the primary sources of uncertainty in yield predictions in the Northern Hemisphere [38,39]. Previous studies combining GCMs with crop process models often overlooked this aspect, leading to divergent simulation outcomes [40,41]. For instance, while some research [42–44] suggests potential yield increases in the main winter wheat production areas of the 3H Plain, others, including Qu et al. [8], indicate that future climate change could adversely affect winter wheat yields [45]. These inconsistencies underscore the importance of precise climate data in crop yield simulations. Our study, therefore, concentrates on enhancing the accuracy of climate projection inputs for crop models to decrease yield projection uncertainties and investigates climate projections over the 3H Plain based on bias-corrected data, aiming to identify the climatic drivers of future agricultural yield changes.

One approach to minimizing uncertainties in CMIP6 projections is using a multi-model ensemble (MME) [36,37]. The MME approach has been proven to offer more reliable confidence and robustness compared to individual models, as errors in simulations and predictions tend to be canceled out when multiple models are considered [46–49]. An alternative approach involves employing a scaling factor derived from comparing the standard deviation of detrended reanalysis data to that of detrended CMIP6 data. The equidistant cumulative distribution function (EDCDF) method has been employed for developing bias-corrected and downscaled climate data. This method, which combines observational data with GCM outputs using a quantile-based mapping approach, has proven more efficient in reducing biases for monthly precipitation and temperature data compared to traditional methods (CDF). The application of bias-corrected CMIP6 data thus significantly contributes to the improved simulation of climate change effects on winter wheat yields.

This paper seeks to integrate agricultural meteorological observations with CMIP6 data to assess the impacts of climate change on winter wheat yields in the 3H Plain, thereby influencing regional climate suitability divisions. Utilizing the DSSAT CERES-Wheat model and six CMIP6 models, this study aims to predict future winter wheat yields in the 3H Plain for the mid- and late 21st century under various scenarios, the flow chart of which is depicted in Figure 1. The specific objectives of this study are to (1) refine the climate projections generated by CMIP6 models to enhance their accuracy and identify the variability in climatic variables; (2) to assess the production of winter wheat in the 3H Plain for the mid- and late 21st century across varied scenarios; (3) to uncover the climatic factors influencing future changes in winter wheat yields; and (4) to offer guidance on the optimal sowing dates, the selection of wheat varieties, and strategic planning for the cultivation of winter wheat.

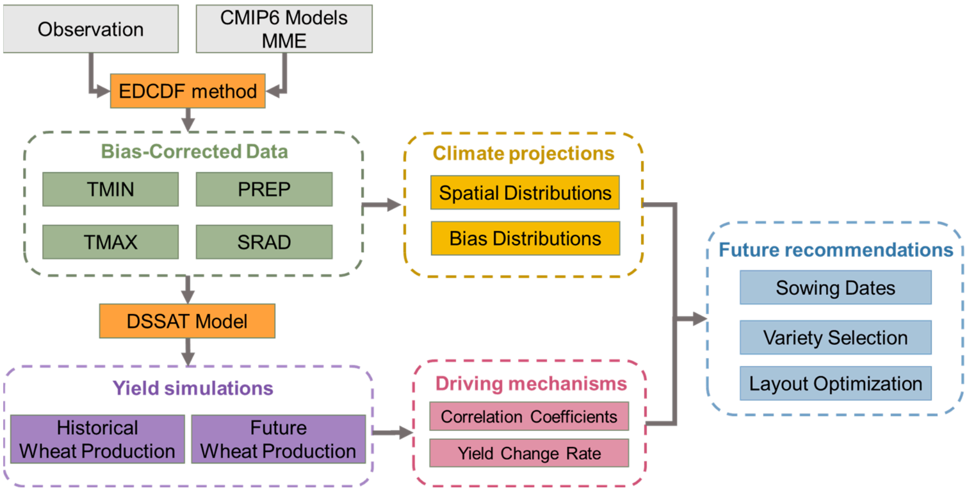

Figure 1. Flow chart of this study.

2. Materials and Methods

2.1. Study Area

The 3H Plain (112.3–120.7° E, 31.1–40.3° N), delimited by the Yellow Sea to the east and covering an area of approximately 350,500 km^2 (Figure 2), exhibits an extratropical monsoon climate. Annual precipitation varies from 430 mm to 1390 mm, with mean temperatures ranging between 8 °C and 15 °C [50]. Notably, over 70% of the annual precipitation occurs during the summer season (June–September) [8], reflecting the region's uneven precipitation distribution. The 3H Plain, with its 140,000 km^2 of arable land [51], is a key grain-producing area in China, contributing over 70% to the country's winter wheat yields. Winter wheat is typically sown in October and harvested in June of the following year.

2.2. Data

This study identified five representative locations for winter wheat analysis, guided by three distinct criteria: (1) the scale of winter wheat cultivation at these sites is substantial and acknowledged by the National Bureau of Statistics of China, making them frequently referenced in crop simulation studies concerning the 3H Plain [8,52,53]; (2) these locations exhibit a range of geographical characteristics, a diversity underscored in the works of Qu et al. [8] and Li et al. [52]; (3) comprehensive and accessible data on winter wheat yields, spanning from 1995 to 2020, are available for these sites (Figure 2). Historical yield data (kg/ha) and phenological information for winter wheat from these sites, spanning from 1995 to 2021, were sourced from the National Bureau of Statistics of China.

Climate simulations from seven CMIP6 models were examined, as summarized in Table 1. For each model, monthly datasets covering temperature, precipitation, the number of wet days, and solar radiation were employed. These datasets were derived from historical simulations spanning from 1995 to 2021 and future projections for the years 2041 to 2100, under two shared socioeconomic pathways (SSP2-4.5 and SSP5-8.5).

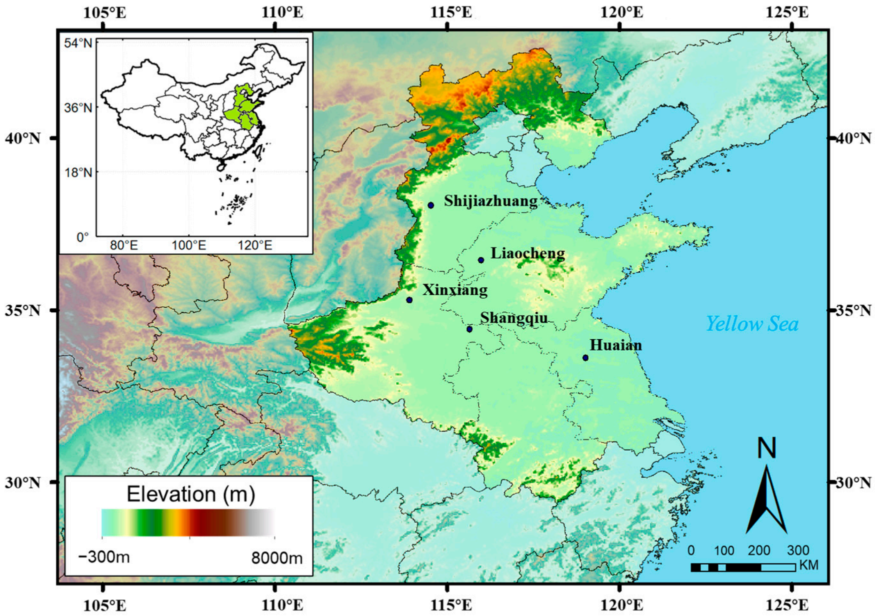

Figure 2. The Huang-Huai-Hai Plain (3H Plain) and the locations of representative sites in this study.

Table 1. Summary of CMIP6 models used in this study.

Model Name	Horizontal Resolutions	Institution/Country
BCC-CSM2-MR	320 × 160	Beijing Climate Center (BCC)/China
MPI-ESM1-2-HR	384 × 192	Max Planck Institute (MPI) for Meteorology/Germany
MIROC6	256 × 128	Model for Interdisciplinary Research on Climate (MIROC)/Japan
GISS-E2-1-G	144 × 90	NASA Goddard Institute for Space Studies (GISS)/USA
IPSL-CM6A-LR	144 × 143	Institute Pierre-Simon Laplace (IPSL)/France
MRI-ESM2-0	320 × 160	Meteorological Research Institute (MRI)/Japan
CESM2	288 × 192	National Center for Atmospheric Research (NCAR)/USA

Given the constraints associated with long-term, ground-based observational data in China, our study opted for reanalysis datasets as the primary source of observations. This decision aligns with the types of data recommended in the official guidelines of the DSSAT. The 0.5° grid monthly temperature, precipitation, and the number of wet days spanning from 1902 to 2020 were sourced from the Climatic Research Unit (CRU TS 4.04) (http://www.cru.uea.ac.uk/data, accessed on 3 February 2024). Additionally, daily solar radiation data for each grid were obtained from the NOAA-CIRES 20th Century Reanalysis V2c (https://www.psl.noaa.gov/data/gridded/data.20thC_ReanV2c.html, accessed on 3 February 2024). These comprehensive meteorological datasets served as the foundational observations for calibrating both the CMIP6 outputs and the winter wheat cultivar simulations.

2.3. Crop Simulation

The DSSAT 4.8 CERES-Wheat model was employed to forecast daily wheat growth, development, and yield for future periods. To operate the model, input datasets were necessary, including data on climate variables, soil properties, management practices, and cultivar coefficients. In this study, the grid served as the fundamental unit for simulation using the DSSAT CERES-Wheat model to project productivity. To precisely evaluate the impact of climate change on winter wheat yields, cultivar coefficients for winter wheat in the 3H Plain were standardized, adhering to the methodology outlined by Li et al. [52]. Detailed general information about the 3H Plain, encompassing genetic coefficients and average planting dates at the five sites, is presented in Tables 2 and 3. Soil characteristics of the 3H Plain, predominantly sandy-loam with medium depth, neutral pH, and low-to-moderate levels of organic carbon, were informed by prior research [54,55]. The planting density was set at 200 plants/m^2, referring to the studies [23,56]. All simulations proceeded under conditions devoid of nitrogen application and reliant on rainfall.

Table 2. Representative site information.

Site	Latitude	Longitude	Sowing Date
Shijiazhuang	38°03′ N	114°26′ E	4-October
Liaocheng	36°26′ N	115°57′ E	15-October
Xinxiang	35°30′ N	113°88′ E	30-October
Shangqiu	34°26′ N	115°38′ E	25-October
Huaian	33°61′ N	119°02′ E	20-October

Table 3. Genetic coefficients in the 3H Plain used for the DSSAT model.

Genetic Coefficients	P1V	P1D	P5	G1	G2	G3	PHT
3H Plain	36.0	63.4	418.8	27.4	28.3	1.66	95

Note: P1V, days at an optimal vernalizing temperature required to complete vernalization; P1D, percentage reduction in the development rate in a photoperiod hour shorter than the threshold relative to that at the threshold; P5, grain-filling phase duration; G1, kernel number per unit canopy weight at anthesis; G2, standard kernel size under optimal conditions; G3, standard, non-stressed dry weight (total, including grain) of a single tiller at maturity; and PHT, interval between successive leaf tip appearances.

In order to validate the accuracy of the crop model parameters across the 3H Plain, the root-mean-square error (RMSE) was employed as a statistical measure. This involved calculating RMSE for the yields predicted by the model against the actual observed yields at five key representative stations, covering the period from 2013 to 2020. A mean RMSE of 10.66% validated the suitability of the genetic coefficients for this study (Figure 3), suggesting that the chosen cultivar is appropriate across the 3H Plain. A pivotal rationale for employing consistent genetic coefficients was to ensure that the results predominantly reflect climate impacts, minimizing the influence of other variables.

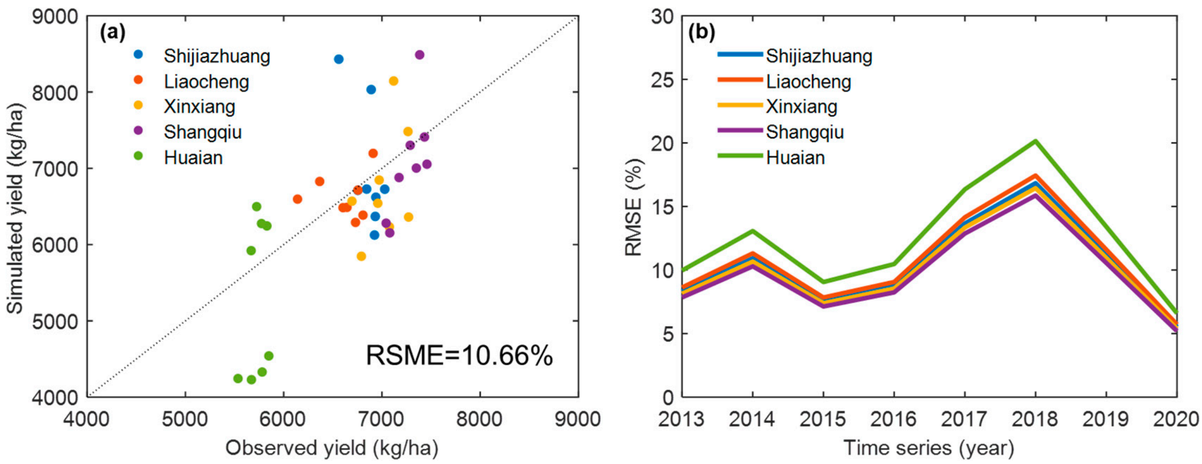

Figure 3. Validation of yields in (**a**) scatter plot and (**b**) time series from 2013 to 2020 at representative sites.

3. Results

3.1. Bias-Corrected Results for Main Climate Factors

Prior to simulating winter wheat yields, the EDCDF method was utilized to adjust the CMIP6-simulated average temperature, precipitation, and solar radiation. This adjustment aims to enhance the accuracy of future climate factor predictions, thereby reducing the uncertainty associated with global ensemble simulations for future yield estimates [57]. The calibration phase used the 1901–1949 period to refine parameters, followed by corrections applied to the main climate factors for the period 1950–2014. Spatial patterns of the bias-corrected climate factors against observations and the original CMIP6 simulations for the benchmark period (1950–2014) are illustrated in Figure 4. The raw CMIP6 simulations generally underestimated temperature and precipitation (Figure 4a,b,d,e) while overestimating solar radiation in the southern parts of the 3H Plain (Figure 4g,h).

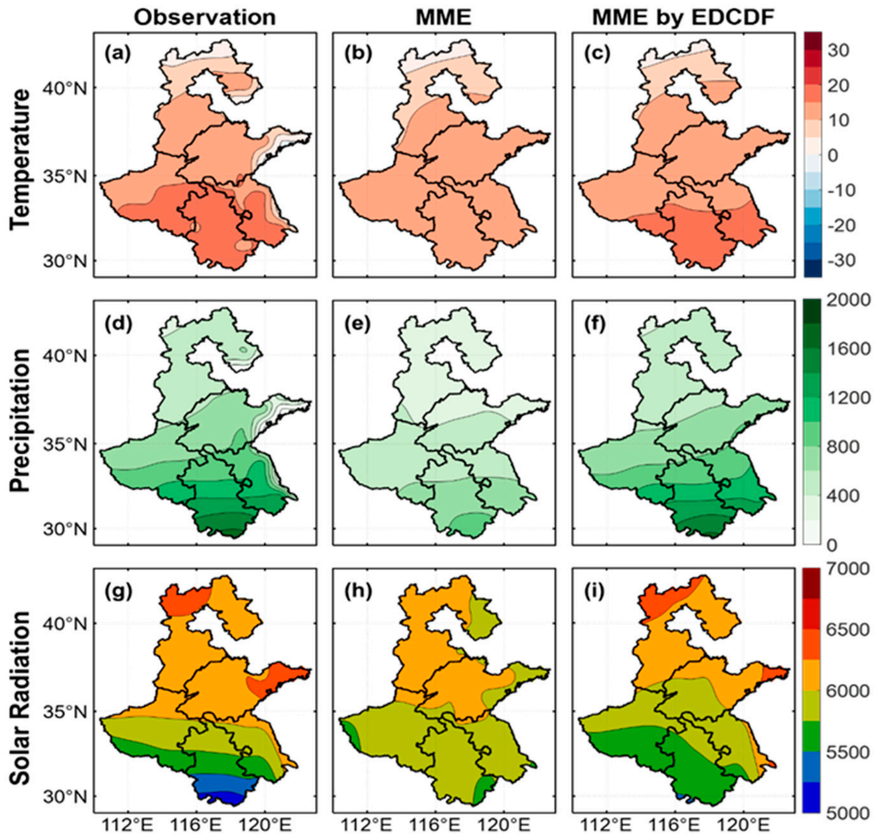

Figure 4. Spatial distributions of (**a**–**c**) temperature (°C), (**d**–**f**) precipitation (mm), and (**g**–**i**) solar radiation (MJ/m^2) over the 3H Plain from 1950 to 2014. The data include observations, the ensemble of raw CMIP6-simulated records, and the bias-corrected results using EDCDF.

The MME approach, a method for reducing uncertainties in CMIP6 data, was also subjected to bias correction using the EDCDF method to further refine CMIP6 data accuracy. The bias-corrected MME results aligned closely with observational data, particularly concerning correcting biases in climate factor values (Figure 4). Specifically, the bias correction addressed the underestimation of temperature in the southern 3H Plain (Figure 4b,c) and the precipitation in the 3H Plain (Figure 4e,f). Moreover, the overestimation of solar radiation in the southern 3H Plain was corrected (Figure 4h,i). The regional average biases for temperature, precipitation, and solar radiation were reduced by 18.3%, 5.6%, and 30.7%, respectively. These results demonstrate that the bias-corrected ensemble of CMIP6 simulations offers an improved representation of spatial patterns for key climate factors, making it suitable to be input into crop model simulations. This finding is consistent with the outcomes reported by Yang et al. [57].

3.2. Climate Variability in Future Scenarios in the 3H Plain

Utilizing the bias-corrected MME results via the EDCDF method, this study adjusted climate factors for the mid-term (2041–2060) and long-term (2081–2100) periods under SSP2-4.5 and SSP5-8.5 scenarios of CMIP6. Figure 5 illustrates the spatial patterns of the projected climate changes in the bias-corrected MME of the CMIP6 models relative to the baseline period (1995–2014). These projections reveal an overall increasing temperature trend across the 3H Plain for both the mid- and late 21st century under both scenarios, with a significant rise in temperature observed under the SSP5-8.5 scenario in the late 21st century (Figure 5a–d).

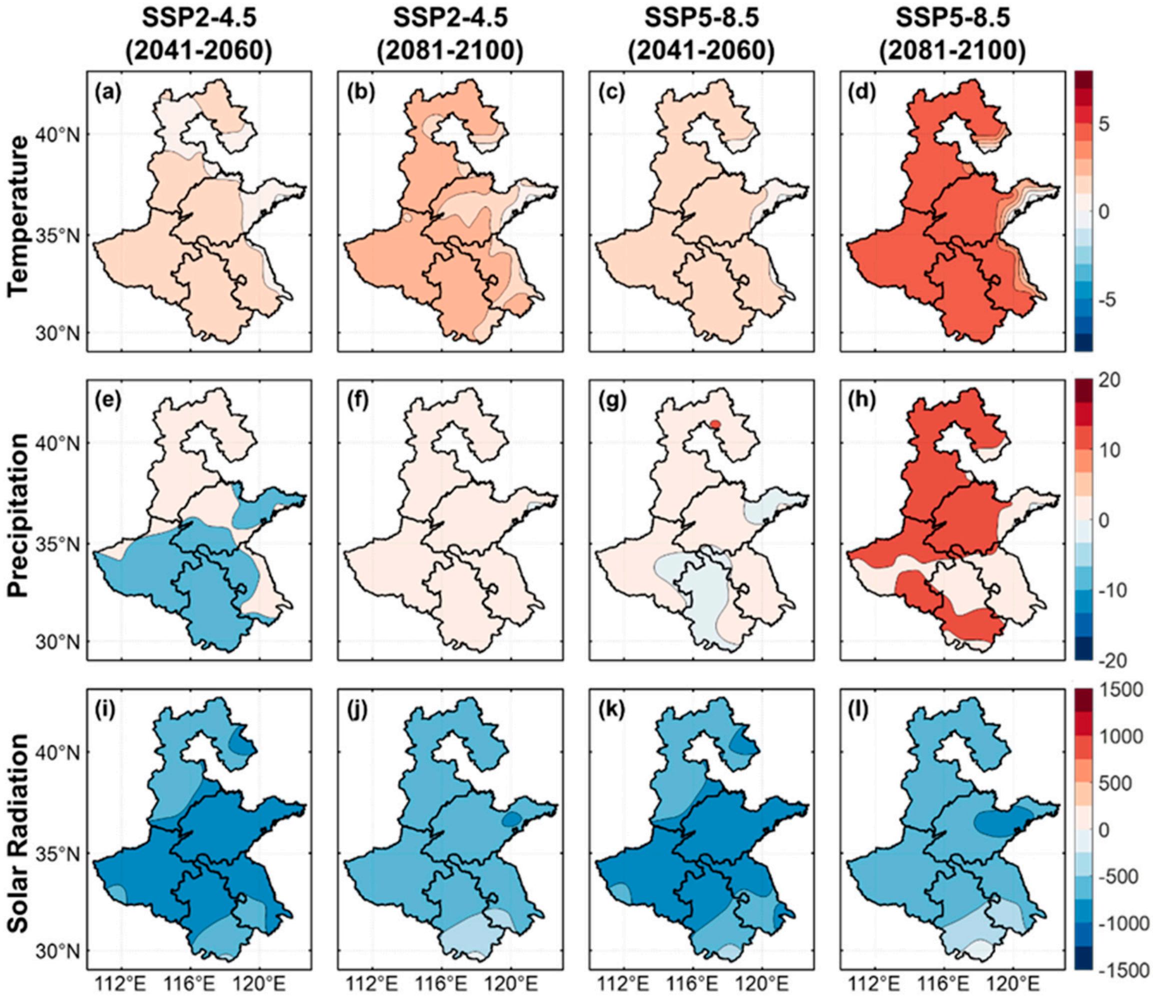

Figure 5. Spatial distributions of multi-model ensemble changes in (**a**–**d**) temperature (°C), (**e**–**h**) precipitation (mm), and (**i**–**l**) solar radiation (MJ/m^2) for the mid- (2041–2060) and late 21st (2081–2100) century across the 3H Plain, relative to the base period (1995–2014), under SSP2-4.5 and SSP5-8.5 scenarios, respectively.

Regarding precipitation, changes during the 2041–2060 period under both scenarios exhibited similar spatial patterns, with decreases observed over the southern and northeast 3H Plain and increases in the northwest (Figure 5e–g). The late 21st century under the SSP5-8.5 scenario showed a slight increase in precipitation, with a more pronounced increase across the 3H Plain from the mid- to late 21st century under the same scenario (Figure 5f–h). These findings aligned with previous research [29,58].

Figure 5 also depicts the spatial patterns of solar radiation across the 3H Plain during the mid- and late 21st century, as simulated under the SSP2-4.5 and SSP5-8.5 scenarios. Solar radiation projections indicate reductions across the 3H Plain in both the mid- and late

21st century under both scenarios (Figure 5i–l), with a smaller decline in the late 21st century, primarily in the central and southern regions of the 3H Plain (Figure 5i–k).

3.3. Impacts of Climate Variability on Winter Wheat Yields in the 3H Plain

Using bias-corrected CMIP6 data under SSP2-4.5 and SSP5-8.5 scenarios, future winter wheat yields were simulated (Figure 6). The SSP2-4.5 scenario predicted broadly high yields in the central 3H Plain for both the 2041–2060 and 2081–2100 periods. Under the SSP5-8.5 scenario, yields in the middle of the 3H Plain were high during the mid-21st century (2041–2060), similar to the SSP2-4.5 scenario, but showed a slight decrease in magnitude and lower yields in the southern 3H Plain during the late 21st century (2081–2100).

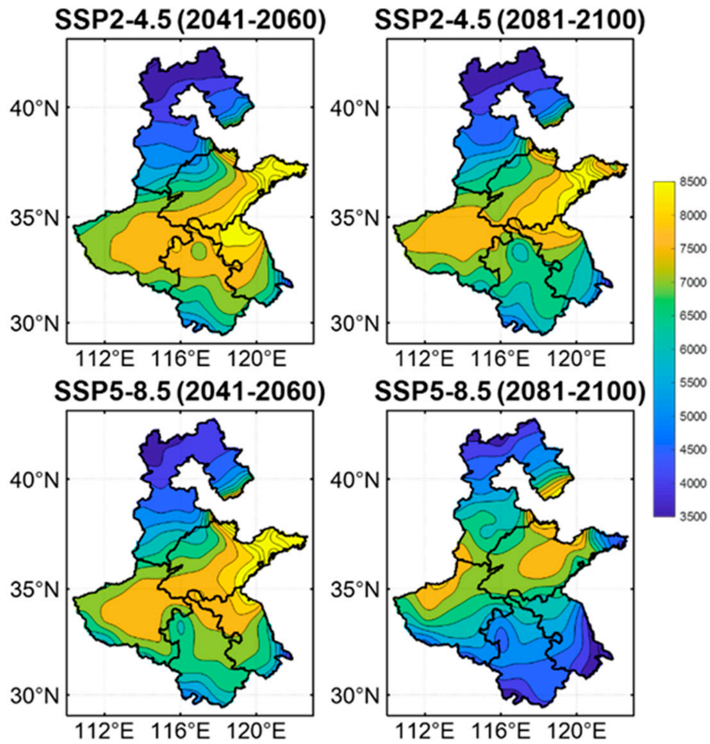

Figure 6. Spatial distributions of winter wheat yield for the mid- (2041–2060) and late 21st (2081–2100) century across the 3H Plain under SSP2-4.5 and SSP5-8.5 scenarios, respectively.

Figure 7 presents the spatial changes in winter wheat yields for the mid- and late 21st century in the 3H Plain relative to the base period under both scenarios. The results indicate a 13% increase in yield across most of the 3H Plain in the mid-21st century under both scenarios. The late 21st century showed an 11.3% increase under SSP2-4.5. However, yields in the central and southeastern 3H Plain exhibited a decreasing trend under both scenarios, with yields under SSP5-8.5 showing a marked decrease of 8.4% south of 36° N and a significant increase of 21.1% north of 36° N.

To further analyze the impact of future climate change on winter wheat yields, correlation coefficients between yields and main climate factors during the growing period were calculated (Figure 8). Under the SSP2-4.5 and SSP5-8.5 scenarios, the future climate factors exhibited varying effects on different regions within the 3H Plain. Under the SSP2-4.5 scenario, precipitation positively affected yields across most of the 3H Plain, with a mean correlation coefficient of 0.35. Winter wheat yields displayed more significant responses to precipitation in high-latitude areas compared to low-latitude areas. In the northern regions above 36° N, the correlation coefficient stood at 0.59, whereas in the southern areas below 36° N, it was only 0.19. These findings suggest that the water deficit for winter wheat in the northern 3H Plain is even more pronounced than in the southern regions.

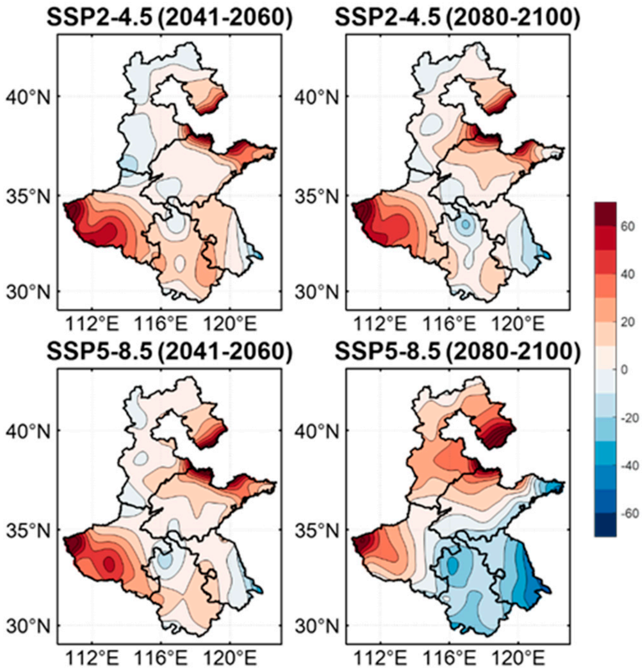

Figure 7. Spatial distributions of winter wheat yield changes (%) for the mid- (2041–2060) and late 21st (2081–2100) century across the 3H Plain, relative to the base period (1995–2014), under SSP2-4.5 and SSP5-8.5 scenarios, respectively.

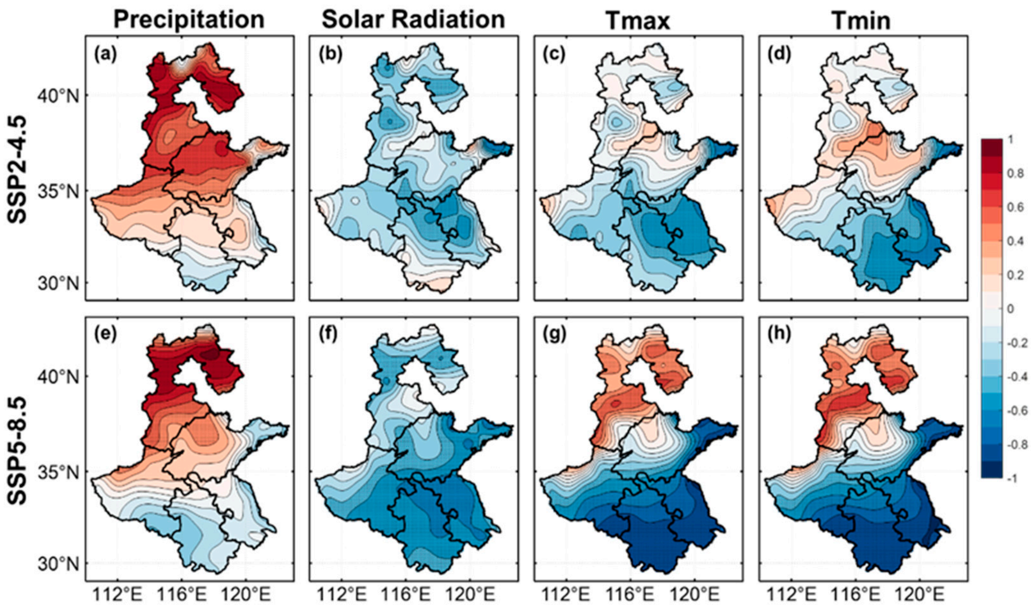

Figure 8. Correlation coefficients between winter wheat yields and (**a**,**e**) precipitation, (**b**,**f**) solar radiation, (**c**,**g**) maximum temperature, and (**d**,**h**) minimum temperature during the growth period of winter wheat for 2041–2100 across the 3H Plain under SSP2-4.5 and SSP5-8.5 scenarios, respectively. The black shade represents the 99% confidence level.

Under the SSP5-8.5 scenario, there was a noticeable shift in the positive value center toward the north. The correlation coefficients between winter wheat yields and temperature (both maximum and minimum) across the 3H Plain indicate a positive relationship in the northern regions and a negative one in the southern areas. This can be attributed to the fact that increased temperature is beneficial for enhancing thermal resources and reducing the risk of cold stress events, which are more prevalent in high-latitude areas [9]. Conversely, higher temperature can lead to a shorter optimal growth period in low-latitude regions where thermal resources are already abundant, resulting in reduced winter wheat yields [59–61].

The magnitude of this effect was more pronounced under the SSP5-8.5 scenario, with a significant correlation coefficient of −0.62 in the southern areas below 36° N and only 0.19 in the northern areas above 36° N. Additionally, most areas within the 3H Plain exhibited a negative correlation between winter wheat yields and solar radiation under both scenarios, with this effect becoming particularly evident under the SSP5-8.5 scenario. It is worth noting that this negative impact of solar radiation on winter wheat yields aligns with findings from Zhang et al. [62], although it is important to acknowledge that this negative impact might be overestimated due to potential inaccuracies in CMIP6 models, such as the underestimation of cloud albedo [63] and the presence of low and mid-level clouds [64].

4. Discussion

The calibration of climate data to improve accuracy is imperative for analyzing the impact of future climate change on winter wheat yields throughout the crop cycle. The observed underestimation of temperature by CMIP6 models in China mirrors similar trends noted in Southeast Asia [63] and the Arctic [64], while contrasting with observations in northern Eurasia [65]. This discrepancy in temperature projections is primarily attributed to the models' handling of cloud representation [31], a critical factor in the accurate simulation of shortwave and longwave cloud forcing, which in turn significantly affects temperature performance [66]. The raw CMIP6 simulations for the benchmark period underestimated precipitation in the 3H Plain, a discrepancy potentially attributable to the models' inadequate representation of terrain features and the representation of air–sea interactions by GCMs [67–69]. Ta et al. [69] identified the inaccurate handling of topography, especially in regions with a complex mountainous terrain, as a common source of precipitation bias. Moreover, the aerosol–cloud interactions and aerosol forced in the emissions simulated by GCMs were found to influence precipitation outcomes [70]. This underestimation aligns with observed discrepancies in extreme precipitation events [71], a pattern also noted in CMIP5 models, which further highlighted the uncertainty in precipitation variability [72]. To address these biases, the MME was corrected using the EDCDF method, which effectively captured the spatial patterns of primary climate factors. This correction reduced the regionally averaged bias for temperature, precipitation, and solar radiation by 18.3%, 5.6%, and 30.7%, respectively. These outcomes echo the findings of Tian et al. [73] and Su et al. [74], demonstrating the efficacy of bias correction in improving model accuracy.

Climate projections suggest an increase in temperature and a decrease in solar radiation throughout the mid- and late 21st century. Consistent with these findings, You et al. [35] reported that temperatures across China are expected to rise by 2.06 °C and 2.66 °C in the mid-term, and by 2.97 °C and 5.62 °C in the long-term, under the SSP2-4.5 and SSP5-8.5 scenarios, respectively. This trend of increasing temperatures aligns with observations in Thailand, where Arunrat et al. [75] confirmed that both maximum and minimum temperatures are projected to rise throughout the 21st century under the SSP2-4.5 and SSP5-8.5 scenarios. In terms of precipitation, forecasts indicate a decrease over the southern and northeast parts of the 3H Plain, with an increase over the northwest during the mid-21st century. Furthermore, a more significant rise in precipitation across the 3H Plain from the mid- to late 21st century is anticipated, primarily driven by changes in thermodynamic factors. Moon et al. [76] specifically noted that convective precipitation over East Asia is expected to significantly increase by the late 21st century under the SSP5-8.5 scenario, showing sensitivity to the rise in temperature. This suggests that extreme precipitation events are likely to occur with higher probability in East Asia under high-emission scenarios.

The yield projections for winter wheat in the 3H Plain show an average increase during the mid- and late 21st century under both the SSP2-4.5 and SSP5-8.5 scenarios. Similar findings have been reported by other studies using CMIP6 models, indicating that winter wheat yields across China are expected to rise [76,77]. These results contrast with those of Lv et al. [42], potentially due to updates and revisions in the CMIP6 data. Specifically, under the SSP5-8.5 scenario, there is a notable yield increase of 21.1% in regions north of 36° N, while a decrease of 8.4% is observed in areas south of 36° N during the late 21st century. This pattern suggests that under higher SSP scenarios, the northern parts of the 3H Plain could become more favorable for winter wheat cultivation compared to the southern regions. These observations align with projections indicating a northward shift in the winter wheat planting boundaries in China [10].

Temperature and precipitation emerge as dominant factors affecting winter wheat yields in the 3H Plain. The relationship between yield and climate change factors exhibits similarities under both SSP2-4.5 and SSP5-8.5 scenarios, with responses to climate change varying by latitude. An anticipated increase in precipitation across most of the 3H Plain under both scenarios suggests improved water resource conditions, potentially reducing drought probability and meeting the water demands of winter wheat in the northern 3H Plain, which has been a major constraint on production [8]. In contrast, the southern 3H Plain, with its relatively abundant water resources, may experience rainfall in excess of the winter wheat's water demand, leading to potential increases in plant diseases, pest outbreaks, and flooding, thus resulting in lower yields [21,78].

Furthermore, the correlation between temperature and winter wheat yields is positive in the northern 3H Plain and negative in the southern region under both scenarios. Increased temperature may alleviate cold stress events threatening the overwintering of crops at higher latitudes but could shorten the optimal growth period for winter wheat in the south, adversely affecting yields [60]. Therefore, regional strategies to enhance crop resilience to warmer temperatures are expected to be most beneficial in the southern 3H Plain. Adaptation measures, such as late sowing of winter wheat or selecting late-maturing cultivars, could extend the growth period, mitigating the adverse effects of rising temperature [79]. Additionally, selecting genotypes with higher heat tolerance than current varieties could offer further adaptation benefits. Notably, winter wheat yields in areas south of 36° N are projected to decrease by 8.4% relative to the baseline period in the late 21st century under the SSP5-8.5 scenario, which is largely due to increased temperature and precipitation changes [80].

In this study, bias-corrected future climate projections were utilized to enhance the accuracy of yield projections; however, uncertainties still persist. The reanalysis datasets served as a critical tool for calibrating both the CMIP6 outputs and the winter wheat cultivar simulations. This approach was primarily adopted due to the constraints associated with the availability of long-term, ground-based observational data in China. While these datasets are an aggregation of interpolated monthly climate anomalies, leveraging extensive networks of weather station observations, it is imperative to acknowledge and consider the inherent discrepancies between reanalysis data and direct observational data [81]. Process-based crop models, such as the DSSAT CERES models, can offer a detailed understanding of the timing, frequency, and intensity of extreme events on crop growth [82], whilst imprecise descriptions of certain processes can introduce uncertainties into the simulation results [83]. For instance, most crop models simulate the effects of high temperature on leaf senescence rather than directly modeling damage to reproductive organs and processes [84,85]. Ongoing research on the impact of extreme events on crop yield failures and the effectiveness of crop models in addressing these challenges warrants further attention [84].

5. Conclusions

This study investigated the impacts of future climate change on winter wheat yields in the 3H Plain using a crop process model and bias-corrected climate projections under SSP2-4.5 and SSP5-8.5 scenarios for the periods 2041–2060 and 2081–2100. The key findings are summarized as follows:

(1) By applying the EDCDF method for bias correction, the regionally averaged discrepancies in temperature, precipitation, and solar radiation across the 3H Plain were

significantly reduced by 18.3%, 5.6%, and 30.7%, respectively. Compared to the reference climate period of 1995–2014, forecasts suggest a general uptrend in temperatures and a downtrend in solar radiation throughout the 3H Plain over the mid- to late 21st century under both SSP scenarios. Furthermore, precipitation levels are anticipated to decline in the southern and northeast parts of the 3H Plain during the mid-21st century, but an overall rise across the plain is expected from the mid- to late 21st century.

(2) The model projections indicate an anticipated average uplift in winter wheat yields by 13% in the mid-21st century under both SSP2-4.5 and SSP5-8.5 scenarios. Moving into the late 21st century, the yield increases are forecasted at 11.3% under SSP2-4.5 and 3.6% under SSP5-8.5. Particularly under the SSP5-8.5 scenario, in the late 21st century, a pronounced disparity in yield trends is observed; yields are projected to surge by 21.1% in areas north of 36° N, contrasting with an 8.4% reduction in areas south of 36° N.

(3) Precipitation has been identified as a critical driver behind the yield boosts in the northern parts of the 3H Plain, showing correlation coefficients of 0.59 under SSP2-4.5 and 0.48 under SSP5-8.5. On the other hand, temperature constraints emerge as a significant hindrance to yields in the southern 3H Plain, evidenced by a correlation coefficient of −0.62 under both scenarios.

(4) This investigation highlights a shift in climatic suitability for winter wheat production in the future, with the northern regions of the 3H Plain showing enhanced prospects for yield improvements. To leverage the increased precipitation forecasts, northern areas should refine water management strategies to maximize crop yield potential. Conversely, the southern regions might need to explore adopting heat-resistant wheat varieties or adjusting planting timelines to mitigate yield losses due to rising temperatures.

Author Contributions: Conceptualization and writing of the original draft, Y.X.; software, reviewing, and editing, T.L.; investigation, M.X.; supervision, L.T. and S.S. All authors have read and agreed to the published version of the manuscript.

Funding: This research was funded by the Youth Foundation of Jiangsu Provincial Meteorological Bureau, grant number KQ202306, and the Key Scientific Foundation of Jiangsu Provincial Meteorological Bureau, grant number KZ202302.

Institutional Review Board Statement: Not applicable.

Data Availability Statement: The climatological data that support the findings of this study during manuscript preparation are available from the first author on reasonable request. Historical annual yield data of winter wheat were obtained from the National Bureau of Statistics of China. The observed monthly temperature, precipitation, and number of wet days data were from the Climatic Research Unit (CRU TS 4.04) (http://www.cru.uea.ac.uk/data (accessed on 15 January 2024)). Daily solar radiation data for each grid were obtained from NOAA-CIRES 20th Century Reanalysis V2c (https://www.psl.noaa.gov/data/gridded/data.20thC_ReanV2c.html (accessed on 16 January 2024)). Historical and future climate scenario data were provided by the World Climate Research Program (WCRP) of the Coupled Model Intercomparison Project Phase 6 (CMIP6, https://esgf-node.llnl.gov/search/cmip6/ (accessed on 20 January 2024)).

Acknowledgments: We are grateful to the World Climate Research Program for providing the climate data from the Coupled Model Intercomparison Project Phase 6 (CMIP6).

Conflicts of Interest: The authors declare no conflicts of interest.

References

1. Song, Y.; Chen, D.; Dong, W. Influence of climate on winter wheat productivity in different climate regions of China, 1961–2000. *Clim. Res.* **2006**, *32*, 219–227. [CrossRef]
2. Alexandrov, V.; Hoogenboom, G. The impact of climate variability and change on crop yield in Bulgaria. *Agric. For. Meteorol.* **2000**, *104*, 315–327. [CrossRef]
3. Godden, D.; Batterham, R.; Drynan, R. Climate change and Australian wheat yield. *Nature* **1998**, *391*, 447–448. [CrossRef]

4. Emami, M.; Almassi, M.; Bakhoda, H.; Kalantari, I. Agricultural mechanization, a key to food security in developing countries: Strategy formulating for Iran. *Agric. Food Secur.* **2018**, *7*, 24. [CrossRef]
5. Bannayan, M.; Rezaei, E.E. Future production of rainfed wheat in Iran (Khorasan province): Climate change scenario analysis. *Mitig. Adapt. Strateg. Glob. Chang.* **2014**, *19*, 211–227. [CrossRef]
6. Maghrebi, M.; Noori, R.; Bhattarai, R.; Yaseen, Z.M.; Tang, Q.; Al-Ansari, N.; Mehr, A.D.; Karbassi, A.; Omidvar, J.; Farnoush, H. Iran's agriculture in the anthropocene. *Earth's Future* **2020**, *8*, e2020EF001547. [CrossRef]
7. Tao, F.; Zhang, L.; Zhang, Z.; Chen, Y. Climate warming outweighed agricultural managements in affecting wheat phenology across China during 1981–2018. *Agric. For. Meteorol.* **2022**, *316*, 108865. [CrossRef]
8. Qu, C.-H.; Li, X.-X.; Hui, J.; Qin, L. The impacts of climate change on wheat yield in the Huang-Huai-Hai Plain of China using DSSAT-CERES-Wheat model under different climate scenarios. *J. Integr. Agric.* **2019**, *18*, 1379–1391. [CrossRef]
9. Yue, Y.; Yang, W.; Wang, L. Assessment of drought risk for winter wheat on the Huanghuaihai Plain under climate change using an EPIC model-based approach. *Int. J. Digit. Earth* **2022**, *15*, 690–711. [CrossRef]
10. Sun, Z.; Jia, S.; Lv, A.; Yang, K.; Svensson, J.; Gao, Y. Impacts of climate change on growth period and planting boundaries of winter wheat in China under RCP4. 5 scenario. *Earth Syst. Dyn. Discuss.* **2015**, *6*, 2181–2210.
11. Shang, S.; Zhang, X.; Shang, Z.; Wu, J. Effect of Climate Change on Yield of Winter Wheat in Jiangsu Province. *Agric. Biotechnol.* **2019**, *8*, 224–234.
12. White, J.W.; Hoogenboom, G.; Kimball, B.A.; Wall, G.W. Methodologies for simulating impacts of climate change on crop production. *Field Crops Res.* **2011**, *124*, 357–368. [CrossRef]
13. Chen, C.; Qian, C.; Deng, A.; Zhang, W. Progressive and active adaptations of cropping system to climate change in Northeast China. *Eur. J. Agron.* **2012**, *38*, 94–103. [CrossRef]
14. Lobell, D.B.; Schlenker, W.; Costa-Roberts, J. Climate trends and global crop production since 1980. *Science* **2011**, *333*, 616–620. [CrossRef] [PubMed]
15. Palosuo, T.; Kersebaum, K.C.; Angulo, C.; Hlavinka, P.; Moriondo, M.; Olesen, J.E.; Patil, R.H.; Ruget, F.; Rumbaur, C.; Takáč, J. Simulation of winter wheat yield and its variability in different climates of Europe: A comparison of eight crop growth models. *Eur. J. Agron.* **2011**, *35*, 103–114. [CrossRef]
16. Chen, Q.; Yu, H.; Hou, W.; Fu, W.; Geng, T.; Chen, C. Impacts of climate warming on growth development process and yield of winter wheat in Huang-Huai-Hai region of China. *J. Triticeae Crops* **2014**, *34*, 1363–1372.
17. Tao, F.; Yokozawa, M.; Zhang, Z. Modelling the impacts of weather and climate variability on crop productivity over a large area: A new process-based model development, optimization, and uncertainties analysis. *Agric. For. Meteorol.* **2009**, *149*, 831–850. [CrossRef]
18. Challinor, A.J.; Simelton, E.S.; Fraser, E.D.; Hemming, D.; Collins, M. Increased crop failure due to climate change: Assessing adaptation options using models and socio-economic data for wheat in China. *Environ. Res. Lett.* **2010**, *5*, 034012. [CrossRef]
19. Zhu, X.; Liu, J.; Shi, B.; Zhang, Y. Variation of climate suitability of winter wheat in Central Plains under the condition of climate warming. *Geogr. Res.* **2012**, *31*, 1479–1489.
20. Yang, X.; Chen, F.; Lin, X.; Liu, Z.; Zhang, H.; Zhao, J.; Li, K.; Ye, Q.; Li, Y.; Lv, S. Potential benefits of climate change for crop productivity in China. *Agric. For. Meteorol.* **2015**, *208*, 76–84. [CrossRef]
21. Xu, Y.; Li, T.; Xu, M.; Shen, S.; Hu, Z. Evaluation of the Pacific Decadal Oscillation from 1901 to 2014 in CMIP6 models. *Clim. Res.* **2023**, *90*, 1–15. [CrossRef]
22. Zhang, Z.; Chen, Y.L.X.; Wang, Y.; Niu, B.; Liu, D.L.; He, J.; Hassan, I.; Meng, Q. Impact of climate change and planting date shifts on growth and yields of double cropping rice in southeastern China in future. *Agric. Syst.* **2023**, *205*, 103581. [CrossRef]
23. Xu, Y.; Li, T.; Shen, S.; Xu, G.; Islam, A.R.M.T.; Hu, Z. Effects of cyclic variability in Pacific decadal oscillation on winter wheat production in China. *Int. J. Climatol.* **2021**, *41*, 2239–2252. [CrossRef]
24. Wolf, J.; Evans, L.; Semenov, M.; Eckersten, H.; Iglesias, A. Comparison of wheat simulation models under climate change. I. Model calibration and sensitivity analyses. *Clim. Res.* **1996**, *7*, 253–270. [CrossRef]
25. Fasullo, J.T.; Phillips, A.S.; Deser, C. Evaluation of Leading Modes of Climate Variability in the CMIP Archives. *J. Clim.* **2020**, *33*, 5527–5545. [CrossRef]
26. Eyring, V.; Bony, S.; Meehl, G.A.; Senior, C.A.; Stevens, B.; Stouffer, R.J.; Taylor, K.E. Overview of the Coupled Model Intercomparison Project Phase 6 (CMIP6) experimental design and organization. *Geosci. Model Dev.* **2016**, *9*, 1937–1958. [CrossRef]
27. Zhou, T. Preface to Special Issue on CMIP6 Experiments: Model and Dataset Descriptions. *Adv. Atmos. Sci.* **2020**, *37*, 1033. [CrossRef]
28. Simpkins, G. Progress in climate modelling. *Nat. Clim. Chang.* **2017**, *7*, 684–685. [CrossRef]
29. Yang, X.; Zhou, B.; Xu, Y.; Han, Z. CMIP6 evaluation and projection of temperature and precipitation over China. *Adv. Atmos. Sci.* **2021**, *38*, 817–830. [CrossRef]
30. Chen, H.; Sun, J.; Lin, W.; Xu, H. Comparison of CMIP6 and CMIP5 models in simulating climate extremes. *Sci. Bull.* **2020**, *65*, 1415–1418. [CrossRef] [PubMed]
31. Jiang, D.; Hu, D.; Tian, Z.; Lang, X. Differences between CMIP6 and CMIP5 models in simulating climate over China and the East Asian monsoon. *Adv. Atmos. Sci.* **2020**, *37*, 1102–1118. [CrossRef]
32. Zhu, H.; Jiang, Z.; Li, J.; Li, W.; Sun, C.; Li, L. Does CMIP6 inspire more confidence in simulating climate extremes over China? *Adv. Atmos. Sci.* **2020**, *37*, 1119–1132. [CrossRef]

33. Su, B.; Huang, J.; Mondal, S.K.; Zhai, J.; Wang, Y.; Wen, S.; Gao, M.; Lv, Y.; Jiang, S.; Jiang, T. Insight from CMIP6 SSP-RCP scenarios for future drought characteristics in China. *Atmos. Res.* **2021**, *250*, 105375. [CrossRef]
34. Li, S.-Y.; Miao, L.-J.; Jiang, Z.-H.; Wang, G.-J.; Gnyawali, K.R.; Zhang, J.; Zhang, H.; Fang, K.; He, Y.; Li, C. Projected drought conditions in Northwest China with CMIP6 models under combined SSPs and RCPs for 2015–2099. *Adv. Clim. Chang. Res.* **2020**, *11*, 210–217. [CrossRef]
35. You, Q.; Cai, Z.; Wu, F.; Jiang, Z.; Pepin, N.; Shen, S.S. Temperature dataset of CMIP6 models over China: Evaluation, trend and uncertainty. *Clim. Dyn.* **2021**, *57*, 17–35. [CrossRef]
36. Manning, L.J.; Hall, J.W.; Fowler, H.J.; Kilsby, C.G.; Tebaldi, C. Using probabilistic climate change information from a multimodel ensemble for water resources assessment. *Water Resour. Res.* **2009**, *45*, 2471–2481. [CrossRef]
37. Brunner, L.; Pendergrass, A.G.; Lehner, F.; Merrifield, A.L.; Knutti, R. Reduced global warming from CMIP6 projections when weighting models by performance and independence. *Earth Syst. Dyn.* **2020**, *11*, 995–1012. [CrossRef]
38. Xie, W.; Wang, S.; Yan, X. DTR in Winter Wheat Growing Regions of China: CMIP6 Models Evaluation and Comparation. *Res. Sq.* **2021**. [CrossRef]
39. Xiong, W.; Asseng, S.; Hoogenboom, G.; Hernandez-Ochoa, I.; Robertson, R.; Sonder, K.; Pequeno, D.; Reynolds, M.; Gerard, B. Different uncertainty distribution between high and low latitudes in modelling warming impacts on wheat. *Nat. Food* **2020**, *1*, 63–69. [CrossRef]
40. Asseng, S.; Ewert, F.; Rosenzweig, C.; Jones, J.W.; Hatfield, J.L.; Ruane, A.C.; Boote, K.J.; Thorburn, P.J.; Rötter, R.P.; Cammarano, D. Uncertainty in simulating wheat yields under climate change. *Nat. Clim. Chang.* **2013**, *3*, 827–832. [CrossRef]
41. Rötter, R.P.; Carter, T.R.; Olesen, J.E.; Porter, J.R. Crop–climate models need an overhaul. *Nat. Clim. Chang.* **2011**, *1*, 175–177. [CrossRef]
42. Lv, Z.; Liu, X.; Cao, W.; Zhu, Y. Climate change impacts on regional winter wheat production in main wheat production regions of China. *Agric. For. Meteorol.* **2013**, *171*, 234–248. [CrossRef]
43. Xiao, D.; Li Liu, D.; Wang, B.; Feng, P.; Bai, H.; Tang, J. Climate change impact on yields and water use of wheat and maize in the North China Plain under future climate change scenarios. *Agric. Water Manag.* **2020**, *238*, 106238. [CrossRef]
44. Rashid, M.A.; Jabloun, M.; Andersen, M.N.; Zhang, X.; Olesen, J.E. Climate change is expected to increase yield and water use efficiency of wheat in the North China Plain. *Agric. Water Manag.* **2019**, *222*, 193–203. [CrossRef]
45. Chen, Y.; Zhang, Z.; Tao, F. Impacts of climate change and climate extremes on major crops productivity in China at a global warming of 1.5 and 2.0 °C. *Earth Syst. Dyn.* **2018**, *9*, 543–562. [CrossRef]
46. Kim, H.M.; Webster, P.J.; Curry, J.A. Evaluation of short-term climate change prediction in multi-model CMIP5 decadal hindcasts. *Geophys. Res. Lett.* **2012**, *39*, 10701. [CrossRef]
47. Chen, H.; Sun, J. How the "best" models project the future precipitation change in China. *Adv. Atmos. Sci.* **2009**, *26*, 773–782. [CrossRef]
48. Yu, H.; Wei, Y.; Zhang, Q.; Liu, X.; Huang, J.; Feng, T.; Zhang, M. Multi-model assessment of global temperature variability on different time scales. *Int. J. Climatol.* **2019**, *40*, 273–291. [CrossRef]
49. Konda, G.; Vissa, N.K. Robustness of BSISO and air-sea interactions in the CMIP (Phase-6) models over the North Indian Ocean. *Dyn. Atmos. Ocean.* **2022**, *99*, 101316. [CrossRef]
50. Shirazi, S.Z.; Mei, X.; Liu, B.; Liu, Y. Estimating potential yield and change in water budget for wheat and maize across Huang-Huai-Hai Plain in the future. *Agric. Water Manag.* **2022**, *260*, 107282. [CrossRef]
51. Zhao, Y.; Xiao, D.; Bai, H.; Tang, J.; Liu, D. Future Projection for Climate Suitability of Summer Maize in the North China Plain. *Agriculture* **2022**, *12*, 348. [CrossRef]
52. Li, Y.; Huang, H.; Ju, H.; Lin, E.; Xiong, W.; Han, X.; Wang, H.; Peng, Z.; Wang, Y.; Xu, J.; et al. Assessing vulnerability and adaptive capacity to potential drought for winter-wheat under the RCP 8.5 scenario in the Huang-Huai-Hai Plain. *Agric. Ecosyst. Environ.* **2015**, *209*, 125–131. [CrossRef]
53. Yang, Y.; Watanabe, M.; Zhang, X.; Hao, X.; Zhang, J. Estimation of groundwater use by crop production simulated by DSSAT-wheat and DSSAT-maize models in the piedmont. *Hydrological Processes* **2006**, *20*, 2787–2802. [CrossRef]
54. Jin, Z.; Ge, D.; Chen, H.; Fang, J. Effects of climate change on rice production and strategies for adaptation in southern China. *Clim. Chang. Agric. Anal. Potential Int. Impacts* **1995**, *59*, 307–323.
55. Rosenzweig, C.; Iglesias, A.; Fischer, G.; Liu, Y.; Baethgen, W.; Jones, J.W. Wheat yield functions for analysis of land-use change in China. *Environ. Model. Assess.* **1999**, *4*, 115–132. [CrossRef]
56. Tian, D.; Asseng, S.; Martinez, C.J.; Misra, V.; Cammarano, D.; Ortiz, B.V. Does decadal climate variation influence wheat and maize production in the southeast USA? *Agric. For. Meteorol.* **2015**, *204*, 1–9. [CrossRef]
57. Yang, X.; Wood, E.F.; Sheffield, J.; Ren, L.; Zhang, M.; Wang, Y. Bias Correction of Historical and Future Simulations of Precipitation and Temperature for China from CMIP5 Models. *J. Hydrometeorol.* **2019**, *19*, 609–623. [CrossRef]
58. Shin, Y.; Shin, Y.; Hong, J.; Kim, M.-K.; Byun, Y.-H.; Boo, K.-O.; Chung, I.-U.; Park, D.-S.R.; Park, J.-S. Future projections and uncertainty assessment of precipitation extremes in the Korean peninsula from the cmip5 ensemble with a statistical framework. *Atmosphere* **2021**, *12*, 97. [CrossRef]

59. Liu, S.; Mo, X.; Lin, Z.; Xu, Y.; Ji, J.; Wen, G.; Richey, J. Crop yield responses to climate change in the Huang-Huai-Hai Plain of China. *Agric. Water Manag. Int. J.* **2010**, *97*, 1195–1209. [CrossRef]
60. Zhang, Z.; Sun, S.; Zhang, F.; Guo, S.; Guo, E.; Liu, Z.; Zhao, J.; Zhao, C.; Li, T.; Yang, X. Using estimated radiation in crop models amplified the negative impacts of climate variability on maize and winter wheat yields in China. *Agric. For. Meteorol.* **2022**, *318*, 108914. [CrossRef]
61. Jian, B.; Li, J.; Wang, G.; Zhao, Y.; Huang, J. Evaluation of the CMIP6 marine subtropical stratocumulus cloud albedo and its controlling factors. *Atmos. Chem. Phys.* **2021**, *21*, 9809–9828. [CrossRef]
62. Zhang, X.; Liang, S.; Wang, G.; Yao, Y.; Cheng, J. Evaluation of the Reanalysis Surface Incident Shortwave Radiation Products from NCEP, ECMWF, GSFC, and JMA Using Satellite and Surface Observations. *Remote Sens.* **2016**, *8*, 225. [CrossRef]
63. Li, J.; Liu, Z.; Yao, Z.; Wang, R. Comprehensive assessment of CMIP5 GCMs using observed temperature and precipitation over mainland Southeast Asia. *Int. J. Climatol.* **2019**, *39*, 4139–4153. [CrossRef]
64. Cai, Z.; You, Q.; Wu, F.; Chen, H.W.; Chen, D.; Cohen, J. Arctic Warming Revealed by Multiple CMIP6 Models: Evaluation of Historical Simulations and Quantification of Future Projection Uncertainties. *J. Clim.* **2021**, *34*, 4871–4892. [CrossRef]
65. Miao, C.; Duan, Q.; Sun, Q.; Huang, Y.; Kong, D.; Yang, T.; Ye, A.; Di, Z.; Gong, W. Assessment of CMIP5 climate models and projected temperature changes over Northern Eurasia. *Environ. Res. Lett.* **2014**, *9*, 055007. [CrossRef]
66. IPCC. Summary for Policymakers, in Climate Change 2013: The Physical Science Basis. In *Intergovernmental Panel on Climate Change (IPCC). Summary for Policymakers. In Climate Change 2013—The Physical Science Basis: Working Group I Contribution to the Fifth Assessment Report of the Intergovernmental Panel on Climate Change*; Cambridge University Press: Cambridge, UK, 2014; pp. 1–30. Available online: https://www.ipcc.ch/report/ar5/wg1/ (accessed on 3 February 2024). [CrossRef]
67. Sun, Q.; Miao, C.; Duan, Q. Comparative analysis of CMIP3 and CMIP5 global climate models for simulating the daily mean, maximum, and minimum temperatures and daily precipitation over China. *J. Geophys. Res. Atmos.* **2015**, *120*, 4806–4824. [CrossRef]
68. Gu, H.; Yu, Z.; Wang, J.; Wang, G.; Yang, T.; Ju, Q.; Yang, C.; Xu, F.; Fan, C. Assessing CMIP5 general circulation model simulations of precipitation and temperature over China. *Int. J. Climatol. J. R. Meteorol. Soc.* **2015**, *35*, 2431–2440. [CrossRef]
69. Ta, Z.; Yu, Y.; Sun, L.; Chen, X.; Mu, G.; Yu, R. Assessment of precipitation simulations in Central Asia by CMIP5 climate models. *Water* **2018**, *10*, 1516. [CrossRef]
70. Lin, L.; Wang, Z.; Xu, Y.; Fu, Q. Sensitivity of precipitation extremes to radiative forcing of greenhouse gases and aerosols. *Geophys. Res. Lett.* **2016**, *43*, 9860–9868. [CrossRef]
71. Ou, T.; Chen, D.; Linderholm, H.W.; Jeong, J.H. Evaluation of global climate models in simulating extreme precipitation in China. *Tellus Ser. A-Dyn. Meteorol. Oceanogr.* **2013**, *65*, 19799. [CrossRef]
72. Sun, Q.; Miao, C.; Duan, Q. Projected changes in temperature and precipitation in ten river basins over China in 21st century. *Int. J. Climatol.* **2015**, *35*, 1125–1141. [CrossRef]
73. Tian, J.; Zhang, Z.; Ahmed, Z.; Zhang, L.; Su, B.; Tao, H.; Jiang, T. Projections of precipitation over China based on CMIP6 models. *Stoch. Environ. Res. Risk Assess.* **2021**, *35*, 831–848. [CrossRef]
74. Su, B.; Huang, J.; Fischer, T.; Wang, Y.; Kundzewicz, Z.W.; Zhai, J.; Sun, H.; Wang, A.; Zeng, X.; Wang, G.; et al. Drought losses in China might double between the 1.5 degrees C and 2.0 degrees C warming. *Proc. Natl. Acad. Sci. USA* **2018**, *115*, 10600–10605. [CrossRef] [PubMed]
75. Arunrat, N.; Sereenonchai, S.; Chaowiwat, W.; Wang, C. Climate change impact on major crop yield and water footprint under CMIP6 climate projections in repeated drought and flood areas in Thailand. *Sci. Total Environ.* **2022**, *807*, 150741. [CrossRef]
76. Moon, S.; Ha, K.-J. Future changes in monsoon duration and precipitation using CMIP6. *npj Clim. Atmos. Sci.* **2020**, *3*, 45. [CrossRef]
77. Liu, X.; Chu, B.; Tang, R.; Liu, Y.; Qiu, B.; Gao, M.; Li, X.; Xiao, J.; Sun, H.Z.; Huang, X.; et al. Air quality improvements can strengthen China's food security. *Nat. Food* **2024**, *5*, 158–170. [CrossRef] [PubMed]
78. Zhang, L.; Wang, F.; Song, H.; Zhang, T.; Wang, D.; Xia, H.; Zhai, S.; Liu, Y.; Wang, T.; Wang, Y.; et al. Effects of projected climate change on winter wheat yield in Henan, China. *J. Clean. Prod.* **2022**, *379*, 134734. [CrossRef]
79. Wiik, L. Control of Fungal Diseases in Winter Wheat—Evaluation of Long-Term Field Research in Southern Sweden. Ph.D. Thesis, Swedish University of Agricultural Sciences, Uppsala, Sweden, 2009.
80. Ali, M.G.M.; Ahmed, M.; Ibrahim, M.M.; El Baroudy, A.A.; Ali, E.F.; Shokr, M.S.; Aldosari, A.A.; Majrashi, A.; Kheir, A.M.S. Optimizing sowing window, cultivar choice, and plant density to boost maize yield under RCP8.5 climate scenario of CMIP5. *Int. J. Biometeorol.* **2022**, *66*, 971–985. [CrossRef]
81. Prasad, G.; Singh, S.M.; Patel, C.; Nema, A.K.; Singh, K.K. Impact of Temperature and Solar Radiation on Wheat Crop for Varanasi Region of Uttar Pradesh. *Vayu Mandal* **2019**, *44*, 47–52.
82. Watson, J.; Zheng, B.; Chapman, S.; Chenu, K. Projected impact of future climate on water-stress patterns across the Australian wheatbelt. *J. Exp. Bot.* **2017**, *68*, 5907–5921. [CrossRef]
83. Eitzinger, J.; Thaler, S.; Schmid, E.; Strauss, F.; Ferrise, R. Sensitivities of crop models to extreme weather conditions during flowering period demonstrated for maize and winter wheat in Austria. *J. Agric. Sci.* **2013**, *151*, 813–835. [CrossRef]

84. Feng, P.; Wang, B.; Li Liu, D.; Waters, C.; Yu, Q. Incorporating machine learning with biophysical model can improve the evaluation of climate extremes impacts on wheat yield in south-eastern Australia. *Agric. For. Meteorol.* **2019**, *275*, 100–113. [CrossRef]
85. Schauberger, B.; Archontoulis, S.; Arneth, A.; Balkovic, J.; Ciais, P.; Deryng, D.; Elliott, J.; Folberth, C.; Khabarov, N.; Müller, C. Consistent negative response of US crops to high temperatures in observations and crop models. *Nat. Commun.* **2017**, *8*, 13931. [CrossRef] [PubMed]